HHS Public Access

Author manuscript

Nanoscale. Author manuscript; available in PMC 2020 September 04.

Published in final edited form as:

Nanoscale. 2018 March 29; 10(13): 6113–6124. doi:10.1039/C7NR09269E.

^{64}Cu-Labeled multifunctional dendrimers for targeted tumor PET imaging†

Wenhui Ma[‡,a,b], **Fanfan Fu**[‡,c], **Jingyi Zhu**[d], **Rui Huang**[a], **Yizhou Zhu**[a], **Zhenwei Liu**[a], **Jing Wang**[b], **Peter S. Conti**[a], **Xiangyang Shi**[c,d], **Kai Chen**[a]

[a]Molecular Imaging Center, Department of Radiology, Keck School of Medicine, University of Southern California, Los Angeles, CA 90033, USA.

[b]Department of Nuclear Medicine, Xijing Hospital, The Fourth Military Medical University, Xi'an, Shaanxi 710032, China

[c]College of Chemistry, Chemical Engineering and Biotechnology, Donghua University, Shanghai 201620, China

[d]State Key Laboratory for Modification of Chemical Fibers and Polymer Materials, College of Materials Science and Engineering, Donghua University, Shanghai 201620, China

Abstract

We report the use of multifunctional folic acid (FA)-modified dendrimers as a platform to radiolabel with ^{64}Cu for PET imaging of folate receptor (FR)-expressing tumors. In this study, amine-terminated generation 5 (G5) poly(amidoamine) dendrimers were sequentially modified with fluorescein isothiocyanate (FI), FA, and 1,4,7,10-tetraazacyclododecane-1,4,7,10-tetraacetic acid (DOTA), followed by acetylation of the remaining dendrimer terminal amines. The as-formed multifunctional DOTA-FA-FI-G5·NHAc dendrimers were then radiolabeled with ^{64}Cu *via* the DOTA chelation. We show that the FA modification renders the dendrimers with targeting specificity to cancer cells overexpressing FR *in vitro*. Importantly, the radiolabeled ^{64}Cu-DOTA-FA-FI-G5·NHAc dendrimers can be used as a nanoprobe for specific targeting of FR-overexpressing cancer cells *in vitro* and targeted microPET imaging of the FR-expressing xenografted tumor model *in vivo*. The developed ^{64}Cu-labeled multifunctional dendrimeric nanoprobe may hold great promise to be used for targeted PET imaging of different types of FR-expressing cancer.

Introduction

Over the past several decades, a greater understanding of tumor biology has yielded better clinical care and improved survival for many patients with cancer. Advances in morphological imaging techniques, particularly magnetic resonance imaging (MRI) and

†Electronic supplementary information (ESI) available: Additional experimental results. See DOI: 10.1039/c7nr09269e

chenkai@med.usc.edu, xshi@dhu.edu.cn.
‡These authors contributed equally to this work.

Conflicts of interest

There are no conflicts to declare.

computed tomography (CT), have improved the detection and staging of tumors, as well as the measurement of therapy response. However, a major limitation of morphological imaging techniques is the inability to characterize tumor growth and metabolism, a matter of pathophysiology. Positron emission tomography (PET), one of the rapidly growing techniques in the medical imaging field, creates the metabolic imaging capability, through which biochemical and physiological aberrations, such as receptor overexpression, can be visualized, characterized, and measured non-invasively and in real time prior to the macroscopic anatomical signs of a disease.[1-3]

PET requires the injection of molecular probes in a tested subject in order to acquire the imaging signal. Molecular probes must be radiolabeled with positron-emitting radionuclides prior to administration.[2,4,5] In addition to conventional PET radionuclides, such as ^{18}F and ^{11}C, metallic radionuclides have been utilized to construct PET probes.[6,7] The metallic PET isotopes, such as ^{64}Cu, ^{86}Y, and ^{89}Zr, usually have longer half-lives, allowing the pharmacokinetic evaluation of a PET probe to be accomplished by successive PET imaging in the same subject over several hours or even days.[8-10] Among these metallic radionuclides, ^{64}Cu ($t_{1/2}$ = 12.7 h; β^+ 655 keV, 17.8%) has attracted a great deal of interest because of its intrinsic half-life decay, low β^+ energy, and commercial availability.[11-13]

Various materials, such as small molecules, peptides, proteins, and nanoparticles (NPs), have been utilized as vehicles of PET probes.[14-16] Among these functional materials, NPs are of particular interest.[17] NPs with typical overall dimensions less than several hundred nanometers are able to marvelously interact with various biological molecules, such as enzymes, receptors, and antibodies.[16] In addition, the large surface area to volume ratio renders NPs with the ability to be readily modified with a variety of moieties to reach multiple binding sites.[18] After labeling with a radionuclide, functionalized NPs can serve as a new class of molecular probes for nuclear imaging, such as PET.

Dendrimers are a family of highly branched, monodispersed, synthetic macromolecules with abundant surface functional groups and generation-dependent sizes, molecular weights, and architecture.[19-21] Due to their unique structural characteristics, dendrimers have been considered to be favorable platforms for the construction of multimodal imaging probes.[22] For targeted tumor imaging, one promising approach is to modify dendrimers with specific ligands that can recognize molecular targets on the surface of cancer cells.[23] Various ligands such as small molecules,[24] peptides,[25] and antibodies[26] have been modified onto the surface of dendrimers for targeted imaging of different types of cancer cells. In particular, as one of the most promising cancer-targeting ligands, folic acid (FA) has been known to target folate receptors (FRs) that are important receptors in cancer treatment[27,28] and overexpressed in several human carcinomas, including breast, ovary, kidney, lung, and brain cancer.[29-31] Therefore, the development of an FR-targeted dendrimer-based PET probe is highly demanded, which would allow us to detect FR-targeted tumor physiology early as well as effectively monitor the response to FR-targeted antitumor therapy.

In our previous work, we have successfully conjugated FA onto different NPs for imaging cancer cells by anatomical imaging modalities, such as magnetic resonance (MR) and computed tomography (CT).[24,32] Indeed, we have shown that FR-targeted NPs are able to be

used as an efficient nanoprobe for the anatomical imaging of cancer cells *in vitro* and xenografted tumor models *in vivo via* an active FR-mediated targeting pathway. These promising results stimulated us to explore the feasibility of using FR-targeted NPs for PET imaging of FR-expressing tumors *in vivo*.

In the present study, we have developed a facile approach for generating an FA-modified multifunctional nanoprobe labeled with ^{64}Cu for specific PET imaging of tumors. A generation 5 (G5) poly(amidoamine) (PAMAM) dendrimer was selected because it has a molecular weight of around 28 kDa, rendering its mouse body clearance about several hours,[33] which matches the ^{64}Cu half-life very well. As compared to the lower generation dendrimers, such as G0-G3 dendrimers,[34,35] G5 dendrimers are favorable for higher loading capacity and improved pharmacokinetics.[23] To the best of our knowledge, there is no previous report on the functional PET imaging of FR-expressing tumors by using G5 dendrimer-based NPs. The G5 PAMAM dendrimer was first conjugated with fluorescein isothiocyanate (FI) and FA, and then coupled with 1,4,7,10-tetraazacyclododecane-1,4,7,10-tetraacetic acid (DOTA), followed by acetylation of the remaining dendrimer terminal amines (Scheme 1). The conjugation of the FI dye onto the G5 PAMAM dendrimers facilitated the *in vitro* characterization of functionalized G5 PAMAM dendrimers. The formed DOTA-FA-FI-G5·NHAc dendrimers were characterized *via* different techniques. The cytotoxicity of the dendrimers was evaluated by the 3-(4,5-dimethylthiazol-2-yl)-2,5-diphenyltetrazolium bromide (MTT) cell viability assay. The FR-mediated specific binding of the DOTA-FA-FI-G5·NHAc dendrimers with KB cells (a human epithelial carcinoma cell line) overexpressing high-affinity FR was confirmed by confocal microscopy. In addition, the radiolabeling of multifunctional dendrimers with ^{64}Cu was achieved in ammonium acetate buffer. The resulting ^{64}Cu-DOTA-FA-FI-G5·NHAc dendrimers were then subjected to cellular uptake, small animal microPET, and biodistribution studies. The FR binding specificity of ^{64}Cu-DOTA-FA-FI-G5·NHAc dendrimers was further evaluated by *in vivo* blocking studies.

Experimental

Materials

All chemicals (reagent grade) were obtained from commercial suppliers and used without further purification. Ethylenediamine core amine-terminated G5 PAMAM dendrimers (G5·NH_2) with a polydispersity index less than 1.08 were purchased from Dendritech (Midland, MI). N-Hydroxysuccinimide (NHS) and 1-ethyl-3-(3-dimethylaminopropyl)carbodiimide hydrochloride (EDC) were purchased from J&K Chemical Reagent Co., Ltd (Shanghai, China). Fluorescein isothiocyanate (FI) and FA were obtained from Aldrich (St Louis, MO). Cellulose dialysis membranes (molecular weight cutoff, MWCO = 500 or 10 000) were acquired from Shanghai Yuanye Biotechnology Corporation (Shanghai, China). 2,2′,2″-(10-(2-(2,5-Dioxopyrrolidin-1-yloxy)-2-oxoethyl)-1,4,7,10-tetraazacyclodode-cane-1,4,7-triyl)triacetic acid (DOTA-NHS) was purchased from CheMatech (Dijon, France). Water used in all experiments was purified using a Milli-Q Plus 185 water purification system (Millipore, Bedford, MA) with a resistivity higher than 18 MΩ cm. [^{64}Cu]$CuCl_2$ was obtained from Washington University in

St Louis, MO, USA. Radio-thin layer chromatography (radio-TLC) was performed on MKC18 silica gel 60 Å plates (GE Healthcare, Piscataway, NJ) with NH_4OAc-EDTA solution (2% EDTA and 10% NH_4OAc)/CH_3OH = 1:1 as the eluent. The plates were analyzed for radioactivity using a Bioscan AR2000 imaging scanner (Washington, DC) with WinScan 2.2 software.

Surface modification of G5·NH_2 dendrimers with FI and FA

G5-NH_2 dendrimers were conjugated with FI and FA according to the protocols described in our previous work[36,37] with slight modification. Briefly, G5·NH_2 dendrimers (40.0 mg, 0.0015 mmol) were dissolved in 5 mL of dimethyl sulfoxide (DMSO). Then, FI (2.9 mg, 0.0075 mmol) in DMSO solution (2 mL) was added dropwise into the dendrimer solution under vigorous magnetic stirring at room temperature. The reaction was continued for 24 h. Then, the reaction mixture was dialyzed against phosphate buffered saline (PBS, 3 times, 2 L) and water (3 times, 2 L) through a dialysis membrane with an MWCO of 10 000 for 3 days to remove the excess of reactants, followed by lyophilization to obtain the FI-G5·NH_2 dendrimers.

The resulting FI-G5·NH_2 dendrimers were then conjugated with FA to afford FA-FI-G5·NHAc dendrimers. In brief, in the presence of 10 molar equivalents of EDC (2.7 mg) and NHS (1.68 mg), the carboxyl groups of FA (3.8 mg, dissolved in 2 mL of DMSO) were first activated under vigorous magnetic stirring at room temperature for 3 h. Then, the activated FA (8 molar equivalents of FI-G5·NH_2) was added dropwise into the DMSO solution of the FI-G5·NH_2 dendrimers (0.00146 mmol, 15 mL) under vigorous magnetic stirring at room temperature. The reaction was stopped after 3 days. Then the reaction mixture was processed according to the procedures described above to obtain the FA-FI-G5·NHAc dendrimers.

Surface modification of FA-FI-G5·NH_2 dendrimers with DOTA

The obtained FA-FI-G5·NH_2 dendrimer (39.2 mg) was dissolved in DMSO (10 mL). Then DOTA-NHS with 12 molar equivalents of the dendrimer (11 mg, 3 mL in DMSO) was added into the dendrimer solution under vigorous magnetic stirring. The reaction was stopped after 24 h. And the reaction mixture was purified according to the above-mentioned procedures to obtain DOTA-FA-FI-G5·NH_2 dendrimers.

The remaining amines of the DOTA-FA-FI-G5·NH_2 dendrimers were converted to acetyl groups by reacting with acetic anhydride according to the literature.[33,34] In brief, the DOTA-FA-FI-G5·NH_2 dendrimer (37.7 mg, in 10 mL of water) was mixed with triethylamine (100 μL, 6.0 μmol) under vigorous magnetic stirring for 0.5 h. Subsequently, acetic anhydride (52 μL, 5 μmol) was added dropwise to the above dendrimer/triethylamine mixture solution under vigorous magnetic stirring. After 24 h, the mixture was processed according to the above-mentioned procedures to obtain the DOTA-FA-FI-G5·NHAc dendrimers.

Radiolabeling of DOTA-FA-FI-G5·NHAc dendrimers

[^{64}Cu]Cu$(OAc)_2$ was prepared by adding 37–111 MBq of [^{64}Cu]$CuCl_2$ in 0.1 M HCl into 300 μL of 0.4 M ammonium acetate buffer (pH = 5.5), followed by mixing and incubating

for 15 min at room temperature. The [^{64}Cu]Cu(OAc)$_2$ solution (37–111 MBq) was then added into a solution of the DOTA-FA-FI-G5·NHAc dendrimers (25 nmol dendrimers per mCi ^{64}Cu) dissolved in 0.4 M NH_4OAc (pH = 5.5) solution. The reaction mixture was incubated at 45 °C for 30 min and purified with a PD-10 column (GE Healthcare, Piscataway, NJ). The radioactive fraction containing the ^{64}Cu-DOTA-FA-FI-G5·NHAc dendrimers was collected and passed through a 0.22-μm syringe filter into a sterile vial for use in the following experiments. The radiochemical purity of the ^{64}Cu-DOTA-FA-FI-G5·NHAc dendrimers was determined by radio-TLC.

Stability study of ^{64}Cu-DOTA-FA-FI-G5·NHAc dendrimers

The *in vitro* stability of the ^{64}Cu-DOTA-FA-FI-G5·NHAc dendrimers was tested in mouse serum. In brief, the ^{64}Cu-DOTA-FA-FI-G5·NHAc dendrimers (3.7 MBq) were incubated with 0.5 mL of mouse serum at 37 °C with gentle shaking. After 1, 6, and 20 h of incubation, trifluoroacetic acid was added to the mixture, and the soluble fraction was filtered with a 0.22 μm filter. An aliquot of the solution was then taken and the radiochemical purity was determined by radio-TLC.

Cell lines

Carcinoma cell lines (KB cell line and A549 human lung adenocarcinoma cell line) were obtained from the American Type Culture Collection (Manassas, VA, USA). The KB cells were cultured at 37 °C in a humidified atmosphere containing 5% CO_2 in regular MEM medium (Mediatech Inc., Manassas, VA) and supplemented with 10% heat-inactivated fetal bovine serum (FBS) (Life Technologies, Grand Island, NY), penicillin (100 U mL^{-1}), and streptomycin (100 U mL^{-1}). The A549 cells were maintained at 37 °C in a humidified atmosphere containing 5% CO_2 in F-12K medium (Mediatech Inc., Manassas, VA) and supplemented with 10% heat-inactivated FBS (Life Technologies, Grand Island, NY), penicillin (100 U mL^{-1}), and streptomycin (100 U mL^{-1}).

Cytotoxicity assay

MTT assay was used to quantify the viability of the cells after treated with the DOTA-FA-FI-G5·NHAc dendrimers at various concentrations. Briefly, the KB or A549 cells were seeded into a 96-well plate at an initial density of 1×10^4 cells per well in 200 μL of culture medium. After overnight incubation, the medium was replaced with 200 μL of fresh medium containing PBS (control) or DOTA-FA-FI-G5·NHAc dendrimers at various concentrations (10, 25, 50, 75, 100, and 200 μg mL^{-1}, respectively). After 24 h of incubation at 37 °C in a humidified atmosphere containing 5% CO_2, 20 μL of MTT solution (0.5 mg mL^{-1} in PBS) was added to each well to detect the metabolically active cells. After an additional 4 h of incubation in an incubator at 37 °C, 150 μL of DMSO was added to each well to replace the culture medium and dissolve the insoluble formazan crystals. The assay was carried out according to the manufacturer's instructions. The absorbance of each well was measured using a SpectraMax M2 microplate reader (Molecular Devices Co., Sunnyvale, CA) at 570 nm. The mean and standard deviation of five parallel wells for each sample were reported.

Confocal microscopy

The KB or A549 cells were grown in chamber slides (VWR International LLC, Radnor, PA) with a density of 5×10^4 cells per well for 24 h to allow the cells to attach onto the slides. After washing with serum-free medium for 3 min, the cells in each well were fixed with 4% paraformaldehyde (PFA) for 10 min, and then washed with serum-free medium (3 times, 3 min per wash). The KB or A549 cells were incubated with fresh medium containing PBS (control) or 50 μM of DOTA-FA-FI-G5·NHAc dendrimers at 37 °C in the dark for 4 h, followed by the PBS wash (3 times, 5 min per wash). For the blocking group, the KB cells were co-incubated with 50 μM of DOTA-FA-FI-G5·NHAc dendrimers and 10 mM of free FA. The chamber slides were then mounted with a DAPI (4′,6-di-amidino-2-phenylindole) containing mounting medium, and placed under a Zeiss LSM 510 confocal laser scanning microscope (Carl Zeiss Microscopy, LLC, Thornwood, NY). The cells on the chamber slides were imaged using a 63× oil-immersion objective lens.

Cellular uptake

The cellular uptake study was performed as previously described with some modifications.[8,9,38] In brief, the KB or A549 cells were seeded into a 48-well plate at a density of 2×10^5 cells per well 24 h prior to the experiment. The tumor cells were then incubated with ^{64}Cu-DOTA-FA-FI-G5·NHAc dendrimers (370 kBq per well) at 37 °C for 15, 30, 60, and 120 min, respectiveIy. For the bIocking study, the KB cells were co-incubated with ^{64}Cu-DOTA-FA-FI-G5·NHAc dendrimers and 50 mM of free FA. After incubation, the tumor cells were washed three times with ice-coId PBS and harvested by trypsinization with 0.25% trypsin/0.02% EDTA (Life TechnoIogies, Grand IsIand, NY). The cell suspensions were collected and measured in a PerkinEImer 2480 WIZARD^2 automatic gamma counter (PerkinEImer Inc., WaItham, MA). The celluIar uptake data were presented as the percentage of the totaI input radioactivity after decay correction. The experiments were performed twice with tripllcate wells.

Animal models

All animaI procedures were performed in accordance with and approved by the Animal Ethics Committee of the University of Southern California (USC), Los Angeles, California, USA, and conformed to the guidelines of the USC Institutional Animal Care and Use Committee. Female athymic nude mice (about 4–6 weeks old, with a body weight of 20–25 g) were obtained from the Envigo, Inc. (Livermore, CA). The mice were fed a FA-deficient rodent chow for 2 weeks prior to tumor implantation and maintained on the same diet throughout the study. The KB or A549 tumor xenografts were generated by subcutaneous injection of 5×10^6 tumor cells into the flanks of female athymic nude mice. The tumors were allowed to grow 3–4 weeks until 300–500 mm^3 in volume was achieved. The tumor growth was followed by caliper measurements of the perpendicular dimensions.

MicroPET imaging and blocking study

About 7.4 MBq of ^{64}Cu-DOTA-FA-FI-G5·NHAc dendrimers was intravenously injected into each mouse (n = 6 per group) under isoflurane anesthesia. Five-minute static scans were acquired at 1, 2, 4, and 6 h post-injection (pi), and a ten-minute static scan was acquired at

20 h pi. The images were reconstructed by a two dimensional (2D) ordered-subsets expectation maximum (OSEM) algorithm. The microPET scans and imaging analysis were performed using a rodent scanner (microPET R4 scanner; Siemens Medical Solutions USA, Inc., Knoxville, TN). For each microPET scan, the regions of interest were drawn over the tumor, the normal tissues, and the major organs on the decay-corrected whole-body coronal images. The radioactivity concentration (accumulation) within the tumor, muscle, liver, and kidneys was obtained from the mean value within the multiple regions of interest and then converted to %ID g^{-1}. For *ex vivo* microPET imaging, the mice were euthanized and dissected at 20 h pi of the ^{64}Cu-DOTA-FA-FI-G5·NHAc dendrimers (7.4 MBq). The blood, the tumor, the major organs, and the tissues were collected, and a ten-minute static microPET scan was acquired. For the blocking experiment, mice bearing KB tumors were scanned after the co-injection of ^{64}Cu-DOTA-FA-FI-G5·NHAc dendrimers (7.4 MBq) with 100 μg of free FA per animal.

Biodistribution

The nude mice bearing KB or A549 tumor (n = 6 per group) were injected with 7.4 MBq of ^{64}Cu-DOTA-FA-FI-G5·NHAc dendrimers. At 20 h pi, the mice were euthanized and dissected. The blood, the tumor, the major organs, and the tissues were collected and wet weighed. The radioactivity in the tissues was measured using a PerkinElmer 2480 WIZARD^2 automatic gamma counter (PerkinElmer Inc., Waltham, MA). The results were presented as the percentage injected dose per gram of tissue (%ID g^{-1}). For each mouse, the radioactivity of the tissue samples was calibrated with a known aliquot of the injected activity. The mean uptake (%ID g^{-1}) for a group of animals was calculated with the standard deviation.

Statistical analysis

The quantitative data were expressed as the mean ± SD. The mean values were compared using one-way ANOVA and student's t-test. The P values <0.05 were considered statistically significant, and the data were indicated with a (*) for $p < 0.05$, (**) for$p < 0.01$, and (***) for$p < 0.001$, respectively.

Results and discussion

Synthesis and characterization of multifunctional dendrimers

The G5 dendrimers were used as a nanoplatform to sequentially conjugate with FI, FA, and DOTA through the amine-mediated covalent conjugation. The remaining dendrimer terminal amines were then acetylated to neutralize the surface positive potential of the dendrimers (Scheme 1). The chemical structures of the intermediate product of FA-FI G5·NH_2 and the final product of DOTA-FA-FI-G5·NHAc were characterized by ^{1}H NMR spectroscopy (Fig. 1). Similar to our previous work,[36,37] for the FA-FI-G5·NH_2 dendrimers, characteristic proton peaks related to both FI and FA can be clearly observed (Fig. 1a). Based on the NMR integration, the number of FI and FA moieties attached to each dendrimer molecule was estimated to be 4.8 and 5.2, respectively. The effect of the substitution degree of FA moieties per dendrimer on the targeting ability of the FA-dendrimer conjugate has been published previously.[39] The published data have shown that modification of 5 FA moieties per G5

dendrimer can achieve a saturated targeting ability towards both the FA binding protein and FR-overexpressing cancer cells. Due to the overlapping of the -CH_2-proton signals of DOTA with those of the ethylene backbone of PAMAM dendrimers, we utilized an indirect method as described in our previous work[40,41] to estimate the number of DOTA moieties conjugated onto each G5 dendrimer. Our data show that the number of DOTA moieties attached onto each G5 dendrimer is 9.8, which is slightly less than the initial molar feeding ratio (12 : 1).

UV-Vis spectroscopy was also used to characterize the synthesized dendrimer conjugates (Fig. 2). In contrast to the pristine G5·NH_2 dendrimers that do not display any apparent features in the wavelength range of 250–600 nm due to their aliphatic structure,[42] the synthesized DOTA-FA-FI-G5·NHAc dendrimers apparently show two absorption peaks, one peak at 500 nm (associated with the FI absorption) and the other peak at 280 nm (associated with the FA absorption). This result clearly indicates the successful conjugation of FI and FA onto the surface of dendrimers, in agreement with our previous work.[37]

The size of the pristine G5·NH_2 dendrimers has been reported to be 5.4 nm, which is similar to that of hemoglobin (http://www.dendritech.com). After the modification of FI, FA, and DOTA, and the acetylation of the remaining dendrimer terminal amines, the size of the dendrimer does not have a significant change since only small molecules are attached onto the dendrimer surface. The surface potential of the DOTA-FA-FI-G5·NHAc dendrimers was found to be 9.1 ± 4.4 mV, in agreement with the literature.[36,37] Multifunctional G5 PAMAM dendrimers with a scaffold size of 5.4 nm have a hydrophilic surface, while their branched interior is quite hydrophobic.[43] In addition, their surface potential is close to be neutral after the partial surface functionalization with FI, FA and DOTA, and further full acetylation of the remaining dendrimer terminal amines.[19,37] With these properties of multifunctional G5 dendrimers, the dendrimeric NPs developed in our study can serve as an ideal platform to be labeled with ^{64}Cu for subsequent PET imaging studies.

Cytotoxicity assay

Before applying the formed DOTA-FA-FI-G5·NHAc dendrimers for *in vivo* studies, it is essential to assess their cytotoxicity. After 24-h incubation of the KB or A549 cells with the DOTA-FA-FI-G5·NHAc dendrimers at the particle concentrations of 10, 25, 50, 75, 100, and 200 μg mL^{-1}, respectively, MTT assay was used to evaluate the cell viability. As shown in Fig. 3, the cell viability does not display significant changes after the KB or A549 cells were treated with the DOTA-FA-FI-G5·NHAc dendrimers in the studied concentration range (0–200 μg mL^{-1}) as compared to the PBS control. This result demonstrates that DOTA-FA-FI-G5·NHAc dendrimers are non-cytotoxic even at a high concentration (200 μg mL^{-1}), suggesting that the DOTA-FA-FI-G5·NHAc dendrimers are biocompatible in the given concentration range for *in vivo* applications. Based on our previous study,[31] the concentration of 100–200 μg mL^{-1} is high enough to justify the cytotoxicity of dendrimer-based NPs.

Confocal microscopy

The FI moieties modified onto the dendrimers enable the confocal microscopic tracking of the cellular uptake of DOTA-FA-FI-G5·NHAc dendrimers. The FR-targeted cellular uptake

of the DOTA-FA-FI-G5·NHAc dendrimers to the KB cells was confirmed by confocal microscopy. The confocal microscopic images of the KB cells treated with PBS and the DOTA-FA-FI-G5·NHAc dendrimers are shown in Fig. 4. Apparent fluorescence signals in the cytosol and on the cell surfaces were observed in the KB cells after incubation with the DOTA-FA-FI-G5·NHAc dendrimers, whereas no fluorescence can be detected in the PBS group. In addition, FA (10 mM) was co-incubated with 50 μM of the DOTA-FA-FI-G5·NHAc dendrimers and the KB cells for 4 h to saturate the FR binding sites. No fluorescence can be clearly identified for the blocking group, which is comparable to the case where the KB cells were treated with PBS. To further evaluate the FR binding specificity of the DOTA-FA-FI-G5·NHAc dendrimers, A549, a known FR-negative cell line, [44] was also used. As shown in Fig. 4, significantly lower fluorescence signals were observed in the A549 cells as compared to the KB cells after incubation with the DOTA-FA-FI-G5·NHAc dendrimers, suggesting that the FR-mediated uptake of the DOTA-FA-FI-G5·NHAc dendrimers in the A549 cells is minimal. Altogether, the results from the confocal microscopy study confirm that the DOTA-FA-FI-G5·NHAc dendrimers can specifically bind to FR-positive KB cells.

Radiolabeling and probe stability

Radiolabeling of the DOTA-FA-FI-G5·NHAc dendrimers with ^{64}Cu (n = 6) was achieved in >85% decay-corrected yield with a radiochemical purity of >99% (Table S1 and Fig. S1, ESI†). The specific activity of ^{64}Cu-DOTA-FA-FI-G5·NHAc dendrimers was estimated to be about 1.25 MBq nmol^{-1}. The *in vitro* stability of the ^{64}Cu-DOTA-FA-FI-G5·NHAc dendrimers was studied in mouse serum at physiological temperature (37 °C) for 1, 6, and 20 h. The stability was presented as the percentage of an intact radiolabeled probe based on radio-TLC analysis. As shown in Fig. 5 and Fig. S1 (ESI†), >93.9% of the ^{64}Cu-DOTA-FA-FI-G5·NHAc dendrimers remained as the parent radiolabeled probe after 20 h of incubation at 37 °C in mouse serum, suggesting that the ^{64}Cu-DOTA-FA-FI-G5·NHAc dendrimers are stable in mouse serum within the study period.

Cellular uptake

The cellular uptake of the ^{64}Cu-DOTA-FA-FI-G5·NHAc dendrimers was examined in FR-positive KB and FR-negative A549 tumor cells. The uptake of the ^{64}Cu-DOTA-FA-FI-G5·NHAc dendrimers in KB cells was determined to be 0.49 ± 0.02% during the first hour of incubation. After 2 h of incubation, the uptake of the ^{64}Cu-DOTA-FA-FI-G5·NHAc dendrimers in KB cells significantly increased to 1.11 ± 0.06% of the total input radioactivity (Fig. 6). In the FR-negative A549 cells, the cellular uptake of the ^{64}Cu-DOTA-FA-FI-G5·NHAc dendrimers was observed at a minimal level of the total input radioactivity after 2 h of incubation. The value was determined to be 0.46 ± 0.03% for the A549 cell uptake, which is significantly lower than that for the KB cells (1.11 ± 0.06% and $p < 0.01$). For the KB cell blocking group, the uptake of the ^{64}Cu-DOTA-FA-FI-G5·NHAc dendrimers (0.58 ± 0.04%) was also significantly lower than that for the non-blocking group ($p < 0.01$). The cellular uptake study revealed that the ^{64}Cu-DOTA-FA-FI-G5·NHAc dendrimers strongly bind to the KB cells, but minimally to the A549 cells or the KB cells blocked with

†Electronic supplementary information (ESI) available: Additional experimental results. See DOI: 10.1039/c7nr09269e

free FA, indicating that the ^{64}Cu-DOTA-FA-FI-G5·NHAc dendrimers are specific to FR-expressing KB cells.

MicroPET imaging

The tumor-targeting efficacy and biodistribution of the ^{64}Cu-DOTA-FA-FI-G5·NHAc dendrimers were evaluated in nude mice bearing FR-positive KB tumor xenografts (n = 6 per group) at 1, 2, 4, 6, and 20 h pi with static microPET scans. The FR-negative A549 tumor xenografts were used as a control for comparison. The KB tumors were clearly visible with high contrast to the background at all imaging time points pi of the ^{64}Cu-DOTA-FA-FI-G5·NHAc dendrimers; whereas the FR-negative A549 tumors exhibited a minimal uptake of the ^{64}Cu-DOTA-FA-FI-G5·NHAc dendrimers. The representative decay-corrected coronal slices that contained the tumors at 1, 2, 4, 6, and 20 h pi are shown in Fig. 7. A predominant uptake of the ^{64}Cu-DOTA-FA-FI-G5·NHAc dendrimers was also observed in the mouse liver and the kidneys for both KB and A549 tumor xenografts. Radioactivity accumulations in tumors and the major organs for microPET scans were quantified by measuring the ROIs that comprised the entire organ on the coronal images. The time–activity curves of the KB tumor, the A549 tumor, liver, kidneys, and muscle after injection of the ^{64}Cu-DOTA-FA-FI-G5·NHAc dendrimers are shown in Fig. 8. The KB tumor uptake of the ^{64}Cu-DOTA-FA-FI-G5·NHAc dendrimers was calculated to be 7.03 ± 0.22, 7.59 ± 0.29, 7.02 ± 0.16, 6.12 ± 0.37, and 2.59 ± 0.38%ID g^{-1} at 1, 2, 4, 6, and 20 h pi, respectively. As a function of time, radioactivity was steadily excreted from the liver and the kidneys. The liver uptake values were calculated to be 9.31 ± 0.86, 9.65 ± 0.76, 9.29 ± 0.65, 8.52 ± 0.66, and 6.30 ± 0.45%ID g^{-1} at 1, 2, 4, 6, and 20 h pi, respectively. The kidney uptake values were calculated to be 10.1 ± 0.51, 10.49 ± 0.24, 9.81 ± 0.47, 8.96 ± 0.57, and 7.92 ± 0.21%ID g^{-1} at 1, 2, 4, 6, and 20 h pi, respectively. Accumulation of the ^{64}Cu-DOTA-FA-FI-G5·NHAc dendrimers in most other organs (except for the intestine) was at a very low level. The KB tumor, the A549 tumor, and the major organ uptake of the ^{64}Cu-DOTA-FA-FI-G5·NHAc dendrimers at 4 h pi are summarized in Table 1. The ratio of the KB tumor uptake to the muscle, the liver, and the kidneys uptake at 4 h pi was calculated to be 10.15 ± 0.14, 0.76 ± 0.39, and 0.72 ± 0.26, respectively. For the FR-negative A549 tumor model, the ^{64}Cu-DOTA-FA-FI-G5·NHAc dendrimers exhibited a minimal tumor uptake and a similar uptake in normal organs and tissues as compared to the FR-positive KB tumor model. The A549 tumor uptake of the ^{64}Cu-DOTA-FA-FI-G5·NHAc dendrimers was calculated to be 1.17 ± 0.22, 1.09 ± 0.35, 0.92 ± 0.26, 0.83 ± 0.17, and 0.61 ± 0.18%ID g^{-1} at 1, 2, 4, 6, and 20 h pi, respectively (Fig. 8). The ratio of A549 tumor uptake to muscle, liver, and kidney uptake at 4 h pi was calculated to be 1.46 ± 0.05, 0.11 ± 0.31, and 0.09 ± 0.28, respectively (Table 1).

To further validate the *in vivo* microPET imaging results, we also carried out *ex vivo* microPET imaging at 20 h pi of the ^{64}Cu-DOTA-FA-FI-G5·NHAc dendrimers (Fig. 9). The mice were euthanized and dissected. The blood, the tumor, the major organs, and the tissues were collected and scanned in the microPET scanner. The *ex vivo* evaluation of the excised organs showed a predominant uptake of the ^{64}Cu-DOTA-FA-FI-G5·NHAc dendrimers in the non-blocking KB tumors (Fig. 9a), whereas a significant reduction of the tumor uptake was observed in the A549 group (Fig. 9c). Aside from the KB tumor, liver and kidney uptake of the ^{64}Cu-DOTA-FA-FI-G5·NHAc dendrimers remained higher than the amounts measured

in other major organs. Based on the quantitative analysis of *ex vivo* microPET imaging, the KB tumor, the liver, and the kidney uptake values were calculated to be 2.49 ± 0.28, 6.15 ± 0.36, and 7.81 ± 0.18%ID g^{-1}, respectively, demonstrating that the results from *ex vivo* imaging are consistent with the *in vivo* findings.

Blocking study

The FR specificity of the ^{64}Cu-DOTA-FA-FI-G5·NHAc dendrimers was further achieved by a blocking experiment where the radiolabeled dendrimers were co-injected with free FA (100 μg per animal). The representative decay-corrected coronal slices that contained the KB tumors at 1, 2, 4, 6, and 20 h pi are shown in Fig. 7. The KB tumor uptake of the ^{64}Cu-DOTA-FA-FI-G5·NHAc dendrimers in the presence of free FA (1.02 ± 0.46%ID g^{-1}) was significantly lower than that without the FA blocking (7.02 ± 0.16%ID g^{-1}) ($p < 0.01$) at 4 h pi (Table 1); whereas the uptake of the ^{64}Cu-DOTA-FA-FI-G5·NHAc dendrimers in other major organs (liver, kidneys, and muscle) in the blocking group was minimally altered as compared to that in the non-blocking group (Fig. 8). The results from *ex vivo* microPET imaging further confirmed the *in vivo* findings (Fig. 9). As shown in Fig. 8, the KB tumor uptake in the blocking group is significantly lower than that in the nonblocking group. Based on the quantitative analysis of *ex vivo* microPET imaging, the KB tumor uptake of the ^{64}Cu-DOTA-FA-FI-G5·NHAc dendrimers at 20 h pi in the non-blocking group and blocking group was determined to be 2.49 ± 0.28 and 0.75 ± 0.31%ID g^{-1}, respectively. These results from the blocking studies demonstrated that the ^{64}Cu-DOTA-FA-FI-G5·NHAc dendrimers are able to specifically target FR-expressing tumors.

Biodistribution

The *ex vivo* biodistribution of the ^{64}Cu-DOTA-FA-FI-G5·NHAc dendrimers was examined in KB or A549 tumor bearing mice at 20 h pi. The percentage administered activity (injected dose) per gram of tissue (%ID g^{-1}) is shown in Fig. 10. The biodistribution results were in agreement with the quantitative analyses of *in vivo* and *ex vivo* microPET imaging. At 20 h pi, the KB tumor uptake of the ^{64}Cu-DOTA-FA-FI-G5·NHAc dendrimers reached 2.17 ± 0.12%ID g^{-1}, whereas the A549 tumor uptake of the ^{64}Cu-DOTA-FA-FI-G5·NHAc dendrimers [0.57 ± 0.06%ID g^{-1} ($p < 0.01$)] remained at a minimal level. In addition, the KB tumor uptake of the ^{64}Cu-DOTA-FA-FI-G5·NHAc dendrimers in the blocking group (0.75 ± 0.07%ID g^{-1}) was significantly lower than that in the non-blocking group [2.17 ± 0.12%ID g^{-1} ($p < 0.01$)]. Overall, the ^{64}Cu-DOTA-FA-FI-G5·NHAc dendrimers exhibited a minimal uptake in most organs (<1% ID g^{-1}) at 20 h pi except for the retention in the liver, the kidneys, and the intestine. For the non-blocking group, 6.73 ± 0.52%ID g^{-1} and 7.97 ± 2.06%ID g^{-1} were measured in the liver and the kidneys, respectively.

Previous studies showed that radiolabeled dendrimers can be used for imaging breast and ovarian cancer, where G0-G3 dendrimers were modified with either the antibody or affibody.[34,35] In our study, G5 dendrimers are modified with FA for FR-targeted cancer imaging. Overall, the nanocore platform as well as the functional ligand of our dendrimers are completely different from those previously reported. Thus, we believe the multifunctional dendrimers that we constructed in this study are unique for our specific application of imaging FR-expressing tumors with PET. In addition, to the best of our knowledge, very few

studies have been reported regarding the FR-targeted NPs for PET imaging. For example, a study showed that FA-conjugated micelles can be used for FR-targeted PET imaging.[30] However, due to the *in vivo* instability, the FA-conjugated micelles exhibit a significant radioactivity uptake in normal organs, such as the liver (21.5 ± 2.9%ID g^{-1} at 24 h pi) and the lungs (10.8 ± 1.4%ID g^{-1} at 24 h pi), resulting in low-imaging contrast and undesirable radiation doses to normal organs; whereas in our study, we demonstrated that >93.9% of the ^{64}Cu-DOTA-FA-FI-G5·NHAc dendrimers remained as the parent probe after 20 h of incubation at 37 °C in mouse serum, suggesting that the ^{64}Cu-DOTA-FA-FI-G5·NHAc dendrimers are quite stable in mouse serum. Furthermore, we not only achieved a very good KB tumor uptake of ^{64}Cu-DOTA-FA-FI-G5·NHAc dendrimers at 20 h post-injection (2.17 ± 0.12%ID g^{-1}), but we also accomplished a lower nonspecific distribution of ^{64}Cu-DOTA-FA-FI-G5·NHAc dendrimers in the normal organs, such as the liver (6.73 ± 0.52%ID g^{-1}). As a result, we believe our study has demonstrated that the ^{64}Cu-DOTA-FA-FI-G5·NHAc dendrimers, as novel biomaterials, display improved imaging contrast and more favorable pharmacokinetic profiles for tumor imaging as compared to the reported NPs.

It is noteworthy that small molecule-based FA derivatives have been radiolabeled with short half-life isotopes, such as ^{68}Ga and ^{18}F, for FR-targeted cancer imaging.[45,46] For example, a recent study showed that a NOTA-containing FA analog can be labeled with Al^{18}F for FR-targeted PET imaging.[46] As compared to the small molecule-based probes, the FA-loaded dendrimer offers increased target binding efficiency and circulation time, and better potential for multimodality imaging and “all-in-one” theranostic applications.[16] In addition, as compared to the short half-life radiolabeled probes, ^{64}Cu-labeled dendrimers allow PET imaging in the same subject at longer time points after injection, facilitating disease diagnosis and evaluation procedures.

In this proof-of-concept study, we chose DOTA as a chelator for ^{64}Cu labeling. DOTA is a commercially available chelator, and a number of ^{64}Cu-DOTA NPs have been exploited for tumor imaging.[15,16,47] However, it is known that a high and prolonged liver uptake may be problematic for the ^{64}Cu-DOTA probes, which was suggested to be the slow dissociation of ^{64}Cu from the DOTA chelator, and the subsequent accumulation of ^{64}Cu in non-target tissues and organs such as in the liver.[48] In our microPET imaging and biodistribution studies, we observed a relatively high accumulation and retention of the ^{64}Cu-DOTA-FA-FI-G5·NHAc dendrimers in mouse liver, which may be due to (i) the unescapable trapping of dendrimers by phagocytic cells, and (ii) the unfavorable demetallation of the ^{64}Cu-DOTA complex in mouse liver. To partially circumvent this problem, better chelation systems for ^{64}Cu labeling such as cross-bridged cyclam ligands or sarcophagine (3, 6, 10, 13, 16, 19-hexaazabicyclo[6.6.6]icosane) may enhance the metal-chelate stability, subsequently leading to a better pharmacokinetic profile.[10,49-51] In addition, it cannot be expected that ^{64}Cu can non-specifically bind to the G5 PAMAM dendrimers. Based on the previous report,[52] the binding capability of Cu(II) to G5-NH2 PAMAM dendrimers is very low in the pH range of 2–5. Particularly, the remaining terminal amines of the G5 PAMAM dendrimers have been completely acetylated in our study. Based on our calculation, the amount of DOTA is slightly excessive than that of ^{64}Cu during radiolabeling, leading the ^{64}Cu capture to full completion by DOTA. To further improve the pharmacokinetics of the ^{64}Cu-labeled

dendrimers, an appropriate linker with suitable hydrophilicity, flexibility, length, and charges could also be incorporated.[53-55]

Conclusions

In summary, multifunctional FR-targeted dendrimers were successfully synthesized and radiolabeled with ^{64}Cu for microPET imaging of FR-expressing tumors. The FA modification onto the dendrimers enables specific targeting of the ^{64}Cu-DOTA-FA-FI-G5·NHAc dendrimers to FR-overexpressing cancer cells *in vitro* and FR-positive tumor xenografts *in vivo via* an FA-mediated active targeting pathway. Given the fact that the DOTA chelator is suitable for radiolabeling with other radiometals, such as ^{111}In, ^{90}Y, and ^{177}Lu, the synthesized multifunctional DOTA-FA-FI-G5·NHAc dendrimers may also be used for SPECT imaging (^{111}In) and radiotherapy (^{90}Y and ^{177}Lu). More broadly, taking into consideration the unique structural characteristics of dendrimers that can be further functionalized with other targeting ligands, multifunctional dendrimeric nanoprobes may be developed for targeted imaging and therapy of different types of cancer.

Supplementary Material

Refer to Web version on PubMed Central for supplementary material.

Acknowledgements

This study was supported by the USC Department of Radiology, the National Natural Science Foundation of China (Grant No. 81761148028 and 21773026), and the Science and Technology Commission of Shanghai Municipality (17540712000).

Abbreviations

PET	Positron emission tomography
SPECT	Single photon emission computed tomography
FR	Folate receptor
G5	Generation 5
FA	Folic acid
NPs	Nanoparticles
FI	Fluorescein isothiocyanate
MR	Magnetic resonance
CT	Computed tomography
EDTA	Ethylenediaminetetraacetic acid
TLC	Thin-layer chromatography
DOTA	1,4,7,10-Tetraazacyclododecane-1,4,7,10-tetraacetic acid

MTT	3-(4,5-Dimethylthiazol-2-yl)-2,5-diphenyltetrazolium bromide
PAMAM	Poly(amidoamine)
NHS	*N*-Hydroxysuccinimide
EDC	1-Ethyl-3-(3-dimethylaminopropyl)-carbodiimide hydrochloride
DMSO	Dimethyl sulfoxide
PBS	Phosphate buffered saline
FBS	Fetal bovine serum
PFA	Paraformaldehyde
DAPI	4′,6-Diamidino-2-phenylindole
DIC	Differential interference contrast
EDTA	Ethylenediamine-tetraacetic acid
OSEM	Ordered-subsets expectation maximum
%ID g^{-1}	Percentage injected dose per gram of tissue
iv	Intravenous
pi	Post-injection

Notes and references

1. Massoud TF and Gambhir SS, Genes Dev., 2003, 17, 545–580. [PubMed: 12629038]
2. Chen K and Chen X, Semin. Oncol, 2011, 38, 70–86. [PubMed: 21362517]
3. Weissleder R and Mahmood U, Radiology, 2001, 219, 316–333. [PubMed: 11323453]
4. Ametamey SM, Honer M and Schubiger PA, Chem. Rev, 2008, 108, 1501–1516. [PubMed: 18426240]
5. Chen K and Conti PS, Adv. Drug Delivery Rev, 2010, 62, 1005–1022.
6. Zeglis BM and Lewis JS, Dalton Trans., 2011, 40, 6168–6195. [PubMed: 21442098]
7. Wadas TJ, Wong EH, Weisman GR and Anderson CJ, Chem. Rev, 2010, 110, 2858–2902. [PubMed: 20415480]
8. Li G, Wang X, Zong S, Wang J, Conti PS and Chen K, Mol. Pharmaceutics, 2014, 11, 3938–3946.
9. Chen K, Ma W, Li G, Wang J, Yang W, Yap LP, Hughes LD, Park R and Conti PS, Mol. Pharmaceutics, 2013, 10, 417–427.
10. Chen K, Wang X, Lin WY, Shen CK, Yap LP, Hughes LD and Conti PS, ACS Med. Chem. Lett, 2012, 3, 1019–1023. [PubMed: 24900423]
11. Shokeen M and Anderson CJ, Acc. Chem. Res, 2009, 42, 832–841. [PubMed: 19530674]
12. Ma MT and Donnelly PS, Curr. Top. Med. Chem, 2011, 11, 500–520. [PubMed: 21189129]
13. Hao G, Singh AN, Oz OK and Sun X, Curr. Radiopharm, 2011, 4, 109–121. [PubMed: 22191650]
14. Chen K and Chen X, Curr. Top. Med. Chem, 2010, 10, 1227–1236. [PubMed: 20388106]
15. Xing Y, Zhao J, Shi X, Conti PS and Chen K, Austin J. Nanomed. Nanotechnol, 2014, 2, 10.
16. Xing Y, Zhao J, Conti PS and Chen K, Theranostics, 2014, 4, 290–306. [PubMed: 24505237]
17. Chen F, Ehlerding EB and Cai W, J. Nucl. Med, 2014, 55, 1919–1922. [PubMed: 25413134]
18. Yu MK, Park J and Jon S, Theranostics, 2012, 2, 3–44. [PubMed: 22272217]

19. Chen Q, Li K, Wen S, Liu H, Peng C, Cai H, Shen M, Zhang G and Shi X, Biomaterials, 2013, 34, 5200–5209. [PubMed: 23583039]
20. Fu F, Wu Y, Zhu J, Wen S, Shen M and Shi X, ACS Appl. Mater. Interfaces, 2014, 6, 16416–16425. [PubMed: 25185074]
21. Zhu J, Zheng L, Wen S, Tang Y, Shen M, Zhang G and Shi X, Biomaterials, 2014, 35, 7635–7646. [PubMed: 24927683]
22. Longmire M, Choyke PL and Kobayashi H, Curr. Top. Med. Chem, 2008, 8, 1180–1186. [PubMed: 18855704]
23. Zhao L, Shi X and Zhao J, Drug Delivery, 2017, 24, 81–93. [PubMed: 29124984]
24. Li J, Zheng L, Cai H, Sun W, Shen M, Zhang G and Shi X, Biomaterials, 2013, 34, 8382–8392. [PubMed: 23932250]
25. Sadler K and Tam JP, J. Biotechnol, 2002, 90, 195–229. [PubMed: 12071226]
26. Yamaguchi H and Harada A, Top. Curr. Chem, 2003, 228, 237–258. [PubMed: 21132488]
27. Assaraf YG, Leamon CP and Reddy JA, Drug Resist. Updates, 2014, 17, 89–95.
28. Ledermann JA, Canevari S and Thigpen T, Ann. Oncol, 2015, 26, 2034–2043. [PubMed: 26063635]
29. Campbell IG, Jones TA, Foulkes WD and Trowsdale J, Cancer Res., 1991, 51, 5329–5338. [PubMed: 1717147]
30. Ross JF, Chaudhuri PK and Ratnam M, Cancer, 1994, 73, 2432–2443. [PubMed: 7513252]
31. Weitman SD, Lark RH, Coney LR, Fort DW, Frasca V, Zurawski VR Jr. and Kamen BA, Cancer Res., 1992, 52, 3396–3401. [PubMed: 1596899]
32. Wang H, Zheng L, Peng C, Shen M, Shi X and Zhang G, Biomaterials, 2013, 34, 470–480. [PubMed: 23088841]
33. Sadekar S, Linares O, Noh G, Hubbard D, Ray A, Janat-Amsbury M, Peterson CM, Facelli J and Ghandehari H, Drug Delivery Transl. Res, 2013, 3, 260–271.
34. Wang Y, Miao Z, Ren G, Xu Y and Cheng Z, Chem. Commun, 2014, 50, 12832–12835.
35. Rahmania H, Mutalib A, Ramli M and Levita J, J. Radiat. Res. Appl. Sci, 2015, 8, 91–99.
36. Wang Y, Cao X, Guo R, Shen M, Zhang M, Zhu M and Shi X, Polym. Chem, 2011, 2, 1754–1760.
37. Wang Y, Guo R, Cao X, Shen M and Shi X, Biomaterials, 2011, 32, 3322–3329. [PubMed: 21315444]
38. Chen K, Sun X, Niu G, Ma Y, Yap LP, Hui X, Wu K, Fan D, Conti PS and Chen X, Mol. Imaging Biol, 2012, 14, 96–105. [PubMed: 21360213]
39. Hong S, Leroueil PR, Majoros IJ, Orr BG, Baker JR Jr. and Banaszak Holl MM, Chem. Biol, 2007, 14, 107–115. [PubMed: 17254956]
40. Chen Q, Li K, Wen S, Liu H, Peng C, Cai H, Shen M, Zhang G and Shi X, Biomaterials, 2013, 34, 5200–5209. [PubMed: 23583039]
41. Wen S, Li K, Cai H, Chen Q, Shen M, Huang Y, Peng C, Hou W, Zhu M, Zhang G and Shi X, Biomaterials, 2013, 34, 1570–1580. [PubMed: 23199745]
42. Shi X, Wang S, Sun H and Baker JR, Soft Matter, 2007, 3, 71–74.
43. Qiao Z and Shi X, Prog. Polym. Sci, 2015, 44, 1–27.
44. Wang Y, Wang Y, Xiang J and Yao K, Biomacromolecules, 2010, 11, 3531–3538. [PubMed: 21086982]
45. Aljammaz I, Al-Otaibi B, Al-Hokbany N, Amer S and Okarvi S, Anticancer Res., 2014, 34, 6547–6556. [PubMed: 25368257]
46. Chen Q, Meng X, McQuade P, Rubins D, Lin SA, Zeng Z, Haley H, Miller P, Gonzalez Trotter D and Low PS, Mol. Pharmaceutics, 2016, 13, 1520–1527.
47. Xie J, Chen K, Huang J, Lee S, Wang J, Gao J, Li X and Chen X, Biomaterials, 2010, 31, 3016–3022. [PubMed: 20092887]
48. Boswell CA, Sun X, Niu W, Weisman GR, Wong EH, Rheingold AL and Anderson CJ, J. Med. Chem, 2004, 47, 1465–1474. [PubMed: 14998334]
49. Sun X, Wuest M, Weisman GR, Wong EH, Reed DP, Boswell CA, Motekaitis R, Martell AE, Welch MJ and Anderson CJ, J. Med. Chem, 2002, 45, 469–477. [PubMed: 11784151]

50. Cai H, Li Z, Huang CW, Shahinian AH, Wang H, Park R and Conti PS, Bioconjugate Chem., 2010, 21, 1417–1424.
51. Cai H, Li Z, Huang CW, Park R, Shahinian AH and Conti PS, Nucl. Med. Biol, 2010, 37, 57–65. [PubMed: 20122669]
52. Diallo MS, Christie S, Swaminathan P, Johnson JH Jr. and Goddard WA, Environ. Sci. Technol, 2005, 39, 1366–1377. [PubMed: 15787379]
53. Chen X, Mini-Rev. Med. Chem, 2006, 6, 227–234. [PubMed: 16472190]
54. Haubner R, Wester HJ, Weber WA, Mang C, Ziegler SI, Goodman SL, Senekowitsch-Schmidtke R, Kessler H and Schwaiger M, Cancer Res., 2001, 61, 1781–1785. [PubMed: 11280722]
55. Shi J, Kim YS, Zhai S, Liu Z, Chen X and Liu S, Bioconjugate Chem., 2009, 20, 750–759.

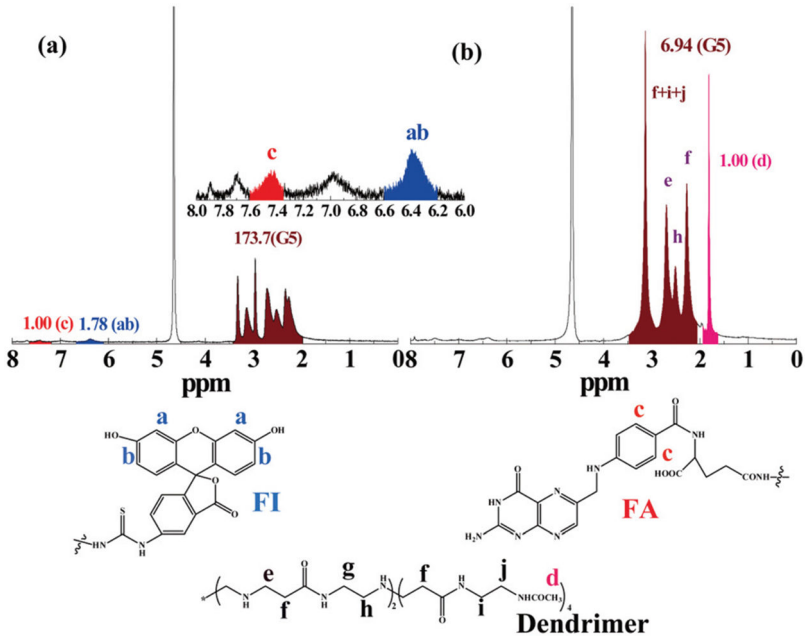

Fig. 1.

^{1}H NMR spectra of FA-FI-G5·NH_2 (a) and DOTA-FA-FI-G5·NHAc (b) dendrimers.

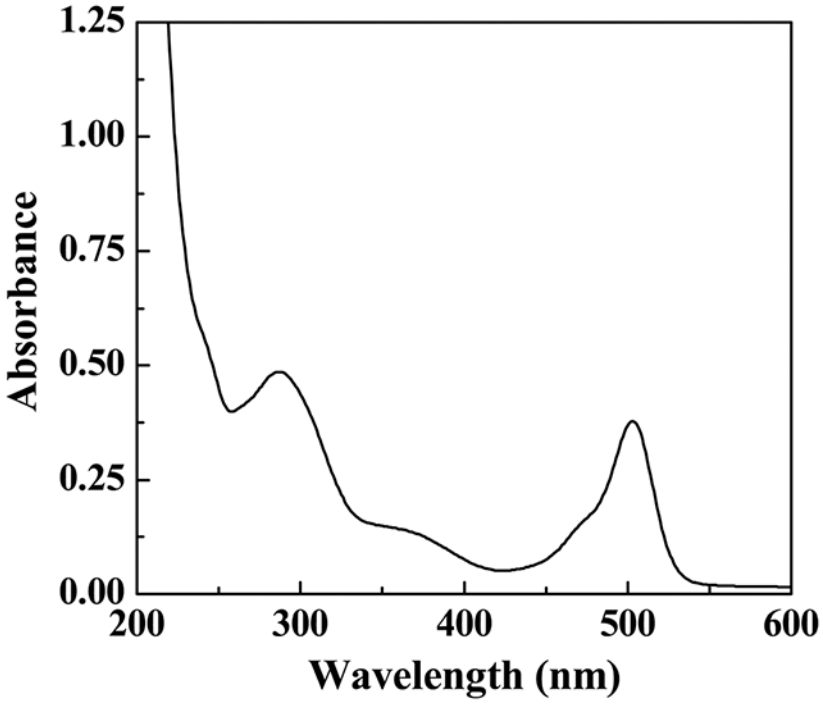

Fig. 2.
UV-Vis spectra of DOTA-FA-FI-G5·NHAc dendrimers dissolved in water.

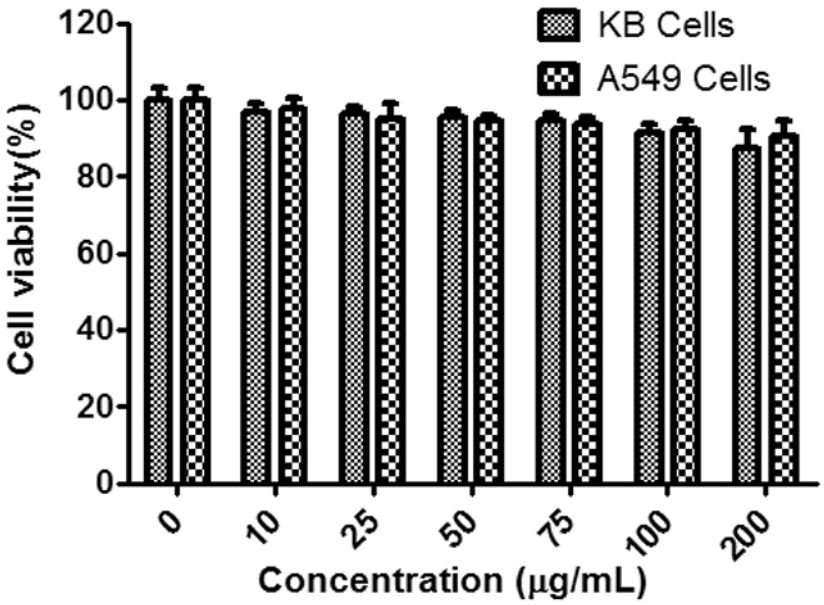

Fig. 3.

MTT assay of KB or A549 cell viability after treatment with DOTA-FA-FI-G5·NHAc dendrimers at a concentration of 0–200 μg mL^{-1} for 24 h. The tumor cells treated with PBS were used as a control.

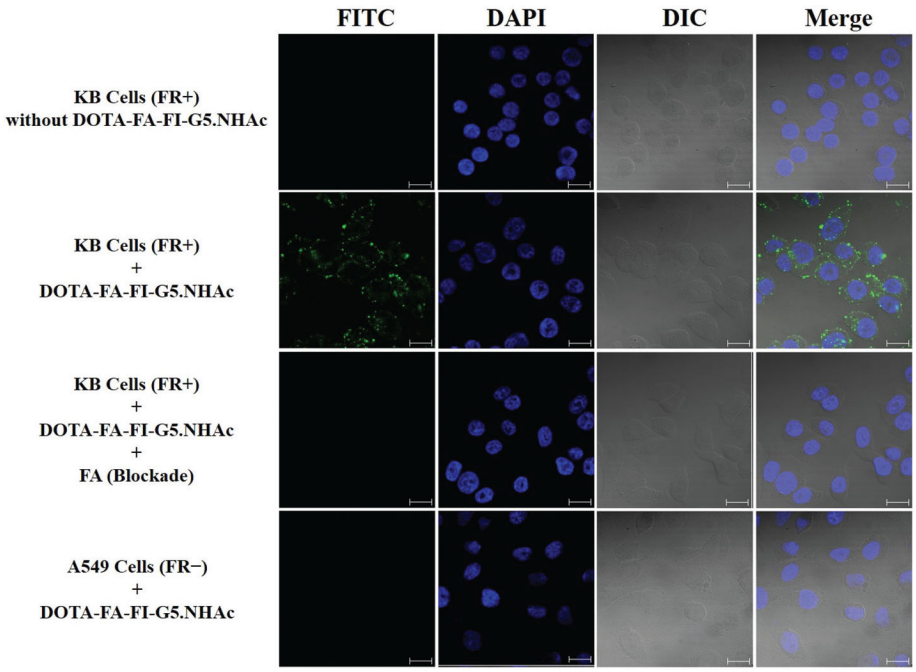

Fig. 4.

Confocal microscopy images of DOTA-FA-FI-G5·NHAc dendrimers with KB cells (FR positive) or A549 cells (FR negative) (magnification 63×; scale bar = 20 μm). The blocking study can be achieved by adding FA.

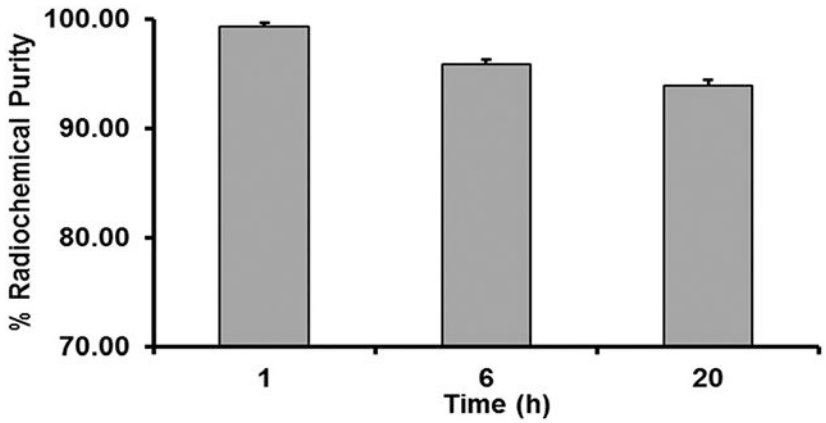

Fig. 5.

Stability of the ^{64}Cu-DOTA-FA-FI-G5·NHAc dendrimers in mouse serum at 37 °C for 1, 6, and 20 h.

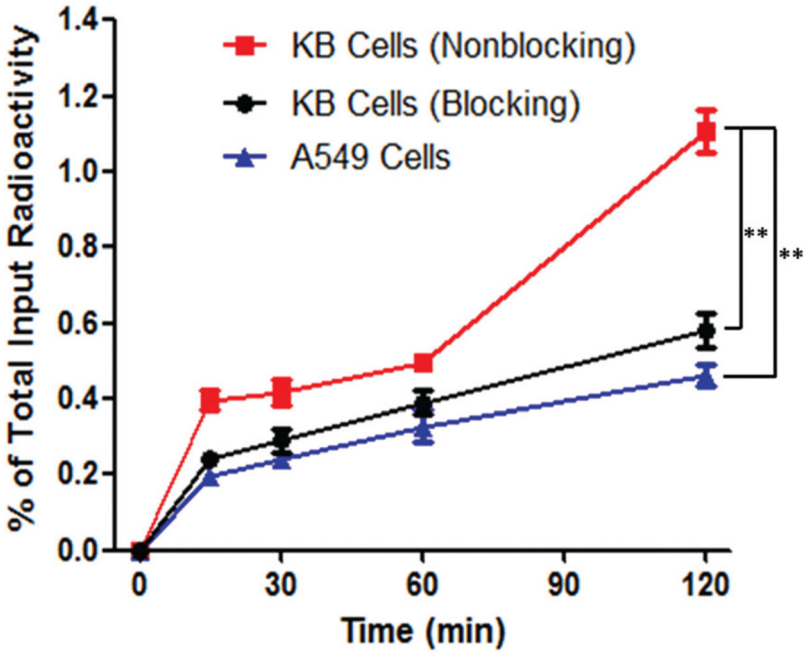

Fig. 6.

Time-dependent cellular uptake of the ^{64}Cu-DOTA-FA-FI-G5·NHAc dendrimers (n = 3 and mean ± SD) using FR-positive KB cells (red line), FR-positive KB cells blocked with free FA (black line), and FR-negative A549 cells (blue line).

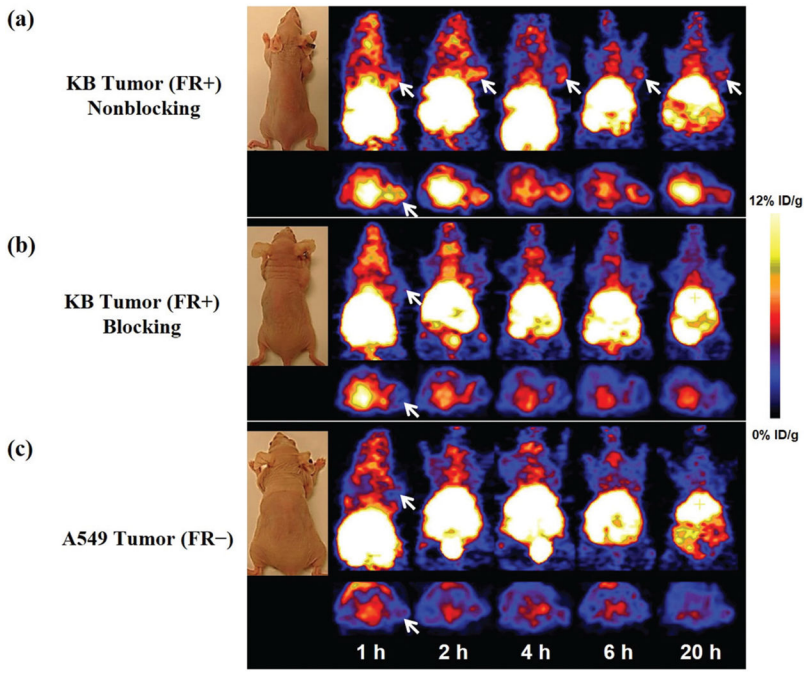

Fig. 7.

MicroPET imaging of the subcutaneous KB tumor or A549 tumor bearing nude mice (n = 6 per group) after intravenous (iv) injection of 7.4 MBq of the ^{64}Cu-DOTA-FA-FI-G5·NHAc dendrimers at 1, 2, 4, 6, and 20 h. (a) Representative decay-corrected whole-body coronal (top) and transverse (bottom) microPET images of nude mice bearing KB tumor. (b) Representative decay-corrected whole-body coronal (top) and transverse (bottom) microPET images of nude mice bearing the KB tumor in a blocking study. The blocking study was performed by i.v. injection of 7.4 MBq of ^{64}Cu-DOTA-FA-FI-G5·NHAc dendrimers with the co-injection of FA (100 μg per mouse) as a blocking agent. (c) Representative decay-corrected whole-body coronal (top) and transverse (bottom) microPET images of nude mice bearing the A549 tumor. The tumors are indicated by arrows.

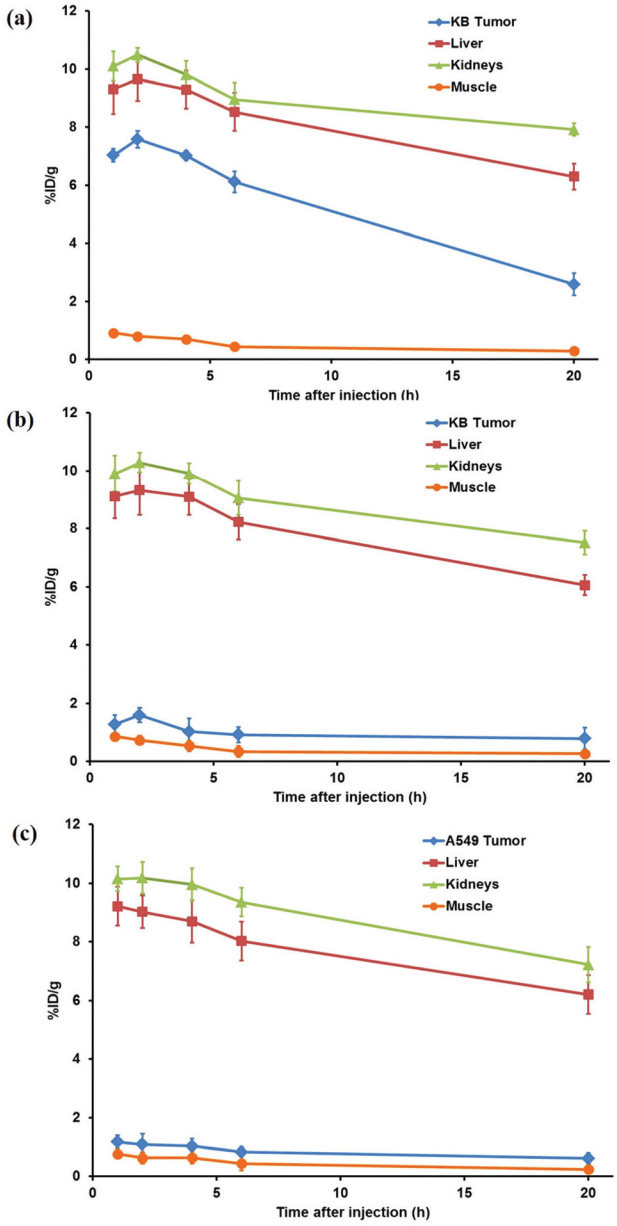

Fig. 8.

Time–activity curves of the tumor, the liver, the kidneys, and the muscle from quantitative microPET imaging analysis of the ^{64}Cu-DOTA-FA-FI-G5·NHAc dendrimers in (a) non-blocking KB tumor model, (b) blocking KB tumor model, and (c) A549 tumor model.

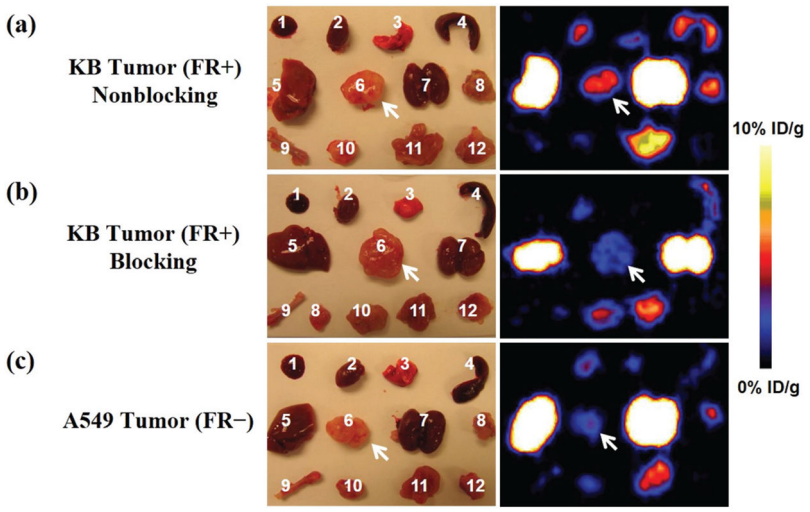

Fig. 9.

Ex vivo microPET imaging of the tumor and normal tissues with the ^{64}Cu-DOTA-FA-FI-G5·NHAc dendrimers (7.4 MBq) after euthanizing the mice at 20 h pi in (a) non-blocking KB tumor model, (b) blocking KB tumor model, and (c) A549 tumor model. (1) Blood, (2) heart, (3) lungs, (4) spleen, (5) liver, (6) tumor, (7) kidneys, (8) pancreas, (9) bone, (10) stomach, (11) intestine, and (12) muscle. The tumors are indicated by arrows.

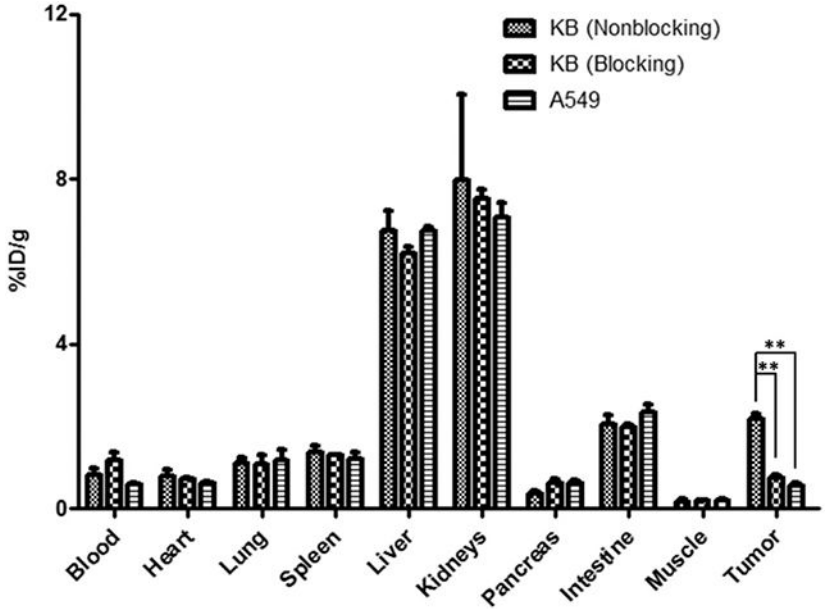

Fig. 10.

Biodistribution of the ^{64}Cu-DOTA-FA-FI-G5·NHAc dendrimers in KB or A549 tumor-bearing athymic nude mice at 20 h pi (n = 6 per group, mean ± SD). Administration of the ^{64}Cu-DOTA-FA-FI-G5·NHAc dendrimers (7.4 MBq) was through iv injection. The blocking study was performed by iv injection of 7.4 MBq of the ^{64}Cu-DOTA-FA-FI-G5·NHAc dendrimers with co-injection of FA (100 μg per mouse) as a blocking agent.

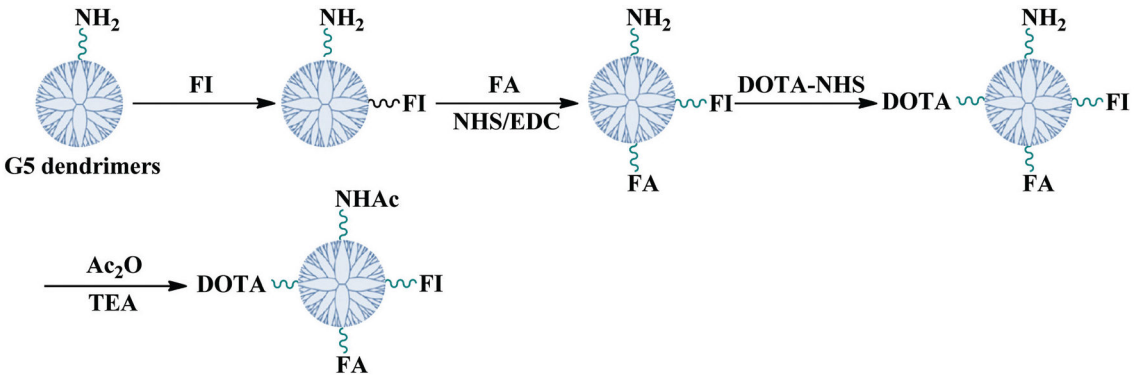

Scheme 1.

Schematic illustration of the synthesis of DOTA-FA-FI-G5·NHAc dendrimers.

Table 1

Decay-corrected biodistribution of the ^{64}Cu-DOTA-FA-FI-G5·NHAc dendrimers at 4 h post-injection in tumor-bearing mice quantified by microPET imaging[a]

Tissue	KB	KB Blockade	A549
Percent injected dose per gram (%ID g^{-1})			
Tumor (T)	7.02 ± 0.16	1.02 ± 0.46	0.92 ± 0.26
Muscle (M)	0.69 ± 0.08	0.53 ± 0.18	0.63 ± 0.21
Liver (L)	9.29 ± 0.65	9.09 ± 0.62	8.69 ± 0.72
Kidneys (K)	9.81 ± 0.47	9.91 ± 0.36	9.96 ± 0.56
Tumor-to-normal tissue uptake ratio			
T/M	10.15 ± 0.14	1.91 ± 0.24	1.46 ± 0.05
T/L	0.76 ± 0.39	0.11 ± 0.19	0.11 ± 0.31
T/K	0.72 ± 0.26	0.10 ± 0.14	0.09 ± 0.28

[a]The results are presented as the mean ± SD (n = 6 per group).